sustainability

MDPI

Article

Experimental Study on Wake Evolution of a 1.5 MW Wind Turbine in a Complex Terrain Wind Farm Based on LiDAR Measurements

Fei Zhao [1], Yihan Gao [2], Tengyuan Wang [3], Jinsha Yuan [1] and Xiaoxia Gao [3,*]

[1] School of Electrical & Electronic Engineering, North China Electric Power University, Baoding 071003, China; zhaofei@ncepu.edu.cn (F.Z.); 51351573@ncepu.edu.cn (J.Y.)
[2] Department of Building Services Engineering, The Hong Kong Polytechnic University, Hong Kong 999077; 19088077g@connect.polyu.hk
[3] Department of Power Engineering, North China Electric Power University, Baoding 071003, China; wojiaowangtengyuan@163.com
* Correspondence: gaoxiaoxia@ncepu.edu.cn; Tel.: +86-0312-7522742; Fax: +86-0312-7522742

Received: 14 January 2020; Accepted: 17 March 2020; Published: 21 March 2020

Abstract: To study the wake development characteristics of wind farms in complex terrains, two different types of Light Detection and Ranging (LiDAR) were used to conduct the field measurements in a mountain wind farm in Hebei Province, China. Under two different incoming wake conditions, the influence of wind shear, terrain and incoming wind characteristics on the development trend of wake was analyzed. The results showed that the existence of wind shear effect causes asymmetric distribution of wind speed in the wake region. The relief of the terrain behind the turbine indicated a subsidence of the wake centerline, which had a linear relationship with the topography altitudes. The wake recovery rates were calculated, which comprehensively validated the conclusion that the wake recovery rate is determined by both the incoming wind turbulence intensity in the wake and the magnitude of the wind speed.

Keywords: wake characteristics; complex terrain; field measurement; wake subsidence; wind shear; LiDAR

1. Introduction

The upstream wind turbines are driven by the incoming wind, which reduce the downstream wind speed and increase the turbulence intensity, and thus, the wakes of upstream wind turbines affect the downstream wind turbines. In addition, numerous scientific studies show that the power loss caused by the wake to the downstream wind turbine is about 40%, and the fatigue load is increased by about 80% [1–3]. In recent years, the amount of flat terrain with high wind speeds that can be developed as wind farms has gradually decreased. Wind farms at high altitudes and complex terrains are becoming a major hot spot for developers. However, the impacts of complex terrain on the operation of wind farms cannot be underestimated, such as the strong wind shear effect, variable atmospheric stability, and surging turbulence levels [4]. Among them, the distribution of wind turbine flow fields under the coupling of terrain and wake has a significant impact on the layout optimization of wind farms [4]. Therefore, the profound understanding of wake evolution in complex terrain is of great significance, which can greatly improve turbines' power generation and reduce fatigue load.

The research methods for wind turbine wake are mainly divided into three categories: wake modeling, numerical simulation and experimental research. Wake models describe the wind speed distribution curve in the far wake region of the wind turbine by using mathematical expressions. Based on the predictable space dimension of wake models, it is divided into one-dimensional wake

models (typically these include the Jensen model [5], Frandsen model [6], etc.), two-dimensional wake models (such as Tian's 2-D Jensen-Cosine model [7] and Gao's 2-D Jensen-Gauss model [8]) and three-dimensional wake models (such as, 3-D Jensen-Gauss model proposed by Sun and Yang [9]). Although the wake model has a very good performance when predicting wake speed, most of the research work on the wake model is mainly focused on flat terrain wind farms and offshore wind farms [10–12]. The development of computer technology has also accelerated the research of numerical simulation on wind turbine wake. Some scholars have achieved good research results. For example, Castellani et al. [13] combined the WindSim CFD numerical tool with supervisory control and data acquisition (SCADA) data to analyze the development characteristics of single-row wind turbines under the combined action of terrain and wake. In the work of Jha et al. [14], the actuator line method was adopted to investigate the effects of turbulence in the wake region on wake recovery under different atmospheric boundary stability levels of two different layout wind farms. Based on GE field experimental data, Nandi et al. [15] used the large eddy simulation method to study the effect of daytime atmospheric turbulence on the non-steady characteristics of local wind speed field and power of the 1.5 MW wind turbine. The effects of atmospheric stability and surface roughness on wind turbines dynamics were explored using a large eddy simulation developed by Churchfield et al. [16]. Meanwhile, Murali et al. [17] used numerical simulation to research the wake development characteristics of wind turbines in complex terrain and the interaction between wakes. Although the numerical simulation can effectively predict the wake characteristics of wind turbines, further verification using field experiments is needed.

A wind tunnel test is a major experimental research method for the study of turbine wakes, which is designed to control experimental conditions (wind speed, direction, turbulence intensity, etc.). Thus, sufficient detailed and accurate data can be obtained. Many scientists have extensively studied wake evolution. Hyvärinen et al. [18] used hot-wire anemometry to collect data and explore the effects of hills and turbulence on the interaction between wakes of multiple wind turbines in a wind tunnel. Dou et al. [19] conducted systematic experimentation to study the wake evolution under different working conditions. Lungo [20] studied the instability of hub vortexes in near-wake flow using fixed-point turbulence measurements. The aeromechanics and wake interferences of wind turbines sited on two-dimensional hills with different slopes were studied by Wei and Ahmet et al. [21], which can be used to optimize the layout of wind turbines sited in complex terrain. However, the limitations of wind tunnels cannot be ignored. The wind tunnel experiment cannot produce the real atmosphere environment, and there are boundary effects and interference of model supports. Moreover, an unmatched Reynolds number results in a decrease in turbine performance [22,23]. Therefore, field measurements are indispensable, as they are able to remove some limitations of the wind tunnel experiments.

Many measurement methods are adopted in field measurements and different methods have their own characteristics. Li et al. [24] conducted a field measurement and two wind-masts were used for measuring the wind speed of the incoming wind and the wind 20 m downstream, respectively. The characteristics of the wake at a fixed downstream distance were studied in this paper. Böhme et al. [25] adopted four wind-scattered masts to assess the impacts of the wake effect. Their study shows that commercial wake models usually underestimate the impacts of turbine wake on power generation. Wind-mast is widely used in field measurements. However, the narrow measurement range makes it impossible to fully measure the entire turbine wake. An instrumented drone that is equipped with a suite of sensors was used in Subramanian et al.'s study [26] and thus, the velocity distribution of the actual wake can be measured. Abraham et al. [27] adopted super-large-scale particle image velocimetry (SLPIV) to investigate the near-wake of a 2.5 MW wind turbine. In this experiment, the tracer particles measured natural snowfall and the device collected abundant data. Recently, LiDAR has been used in field measurement, which can obtain wind speed data in three-dimensional space. Torres et al. [28] conducted a LiDAR field measurement experiment for seven months to investigate the interaction between the wake streams of two wind turbines. Lungo et al. [20] studied

the wake characteristics of a 2 MW wind turbine using three LiDAR methods. Kumer et al. [29] used a LiDAR method to study the turbulent kinetic energy characteristics of the wind turbine wake. In conclusion, wind field measurements are needed to obtain wake data under real conditions. In the experiments of Perdigão 2015 [30] and Perdigão 2017 [31], many experimental studies on the wake characteristics of wind turbines had been carried out and it was proven that two different LiDAR types (Long-range WindScanner and short-range WindScanner) can effectively investigate the wake characteristics of a single wind turbine with a complex terrain, which provides a method guide for future LiDAR measurement experiments. In our previous study [32], the Plan-Position-Indicator mode (PPI) of LiDAR 3D6000 was used to detect the wake interaction characteristics of a single row wind turbines at different altitudes with a complex terrain, and this was combined with the SCADA data to investigate the wind turbine power generation. From the above analysis, it can be concluded that previous research work mainly focused on wake interaction of multiple turbines and wake flow field distribution in wind farms with complex terrain, but the influence of incoming wind characteristics and topography on the wake development characteristics of a single wind turbine is not further quantified. In this instance, the Doppler-Beam-Swing mode (DBS) of WP350 and the Range-Height-Indicator mode (RHI) of 3D6000 are used in this study to obtain the incoming wind data and wake data of a 1.5 MW wind turbine under a complex terrain. Based on the experimental data, the effects of incoming wind shear, wind speed, incoming turbulence intensity and topography on the wake distribution characteristics are quantified. This study aims to analyze the wake distribution characteristics of a single wind turbine under different inflow wind conditions in complex terrain, which will be beneficial to the layout optimization of wind farms and the yaw control of wind turbines.

The content of the article is arranged as follows: Section 2 introduces the experimental site, experimental instruments and wind measurement scheme. The main results and discussions are presented in Section 3, in which the wake characteristics in a vertical height plane, the influence of topographic effects on wake subsidence as well as the wake recovery rate are discussed and analyzed. Conclusions and further recommendations are summarized in Section 4.

2. Set-Up of the LiDAR Measurement Campaign

2.1. Introduction of Experimental Site

The full scale measurement campaign was carried out in a mountain wind farm in Zhangbei County, Hebei Province, China which lasted for 6 months from December 26th, 2018 until May 28th, 2019. The terrain of the wind farm is complex, with an average elevation above 1800 m, which can be observed in Figure 1. Turbine 10-2 indicates the analytic objectives in this wind measurement experiment with a rated power capacity of 1.5 MW, which is located at the highest point of 1884 m. The rotor diameter is 77 m with a hub height of 65 m.

2.2. LiDAR Measurement Scheme

In order to simultaneously investigate the inflow wind condition and the distribution characteristics of the wake speed of a single wind turbine in complex wind farms accurately, two different types of ground-based coherent Doppler LiDAR are used. One is a wind-profile LiDAR, model WP350, and uses its DBS mode to measure the wind profile and turbulence intensity of the wind blowing on the wind turbine at different heights; the other is a three-dimensional scanning LiDAR, model 3D6000, which is used to measure wind speed profiles behind the wind turbine. The 3D6000 mainly has two measurement modes: PPI and RHI. The PPI mode mainly measures the distribution of wind speed on the horizontal plane by changing the azimuth at a fixed elevation angle, while the RHI mode measures the distribution of wind velocity on the vertical plane by varying the elevation angle and fixing the azimuth angle [33,34]. Considering that the focus of this study is the wake field distribution characteristics of the vertical height plane in the wake region under the combined effects of incoming wind conditions and topography, the RHI mode of 3D6000 is more appropriate in this study [30]. Note

that the wind speed used in this experiment is the horizontal wind speed obtained by the inverse calculation of los wind speed, which can be seen in Appendix A. In addition, the signal-noise ratio (SNR) threshold set during data inversion is 10, which means that when the calculated SNR is lower than the set value, the signal at this time is not considered to be the true wind speed signal, and these signals will be removed to ensure the validity of the experimental data.

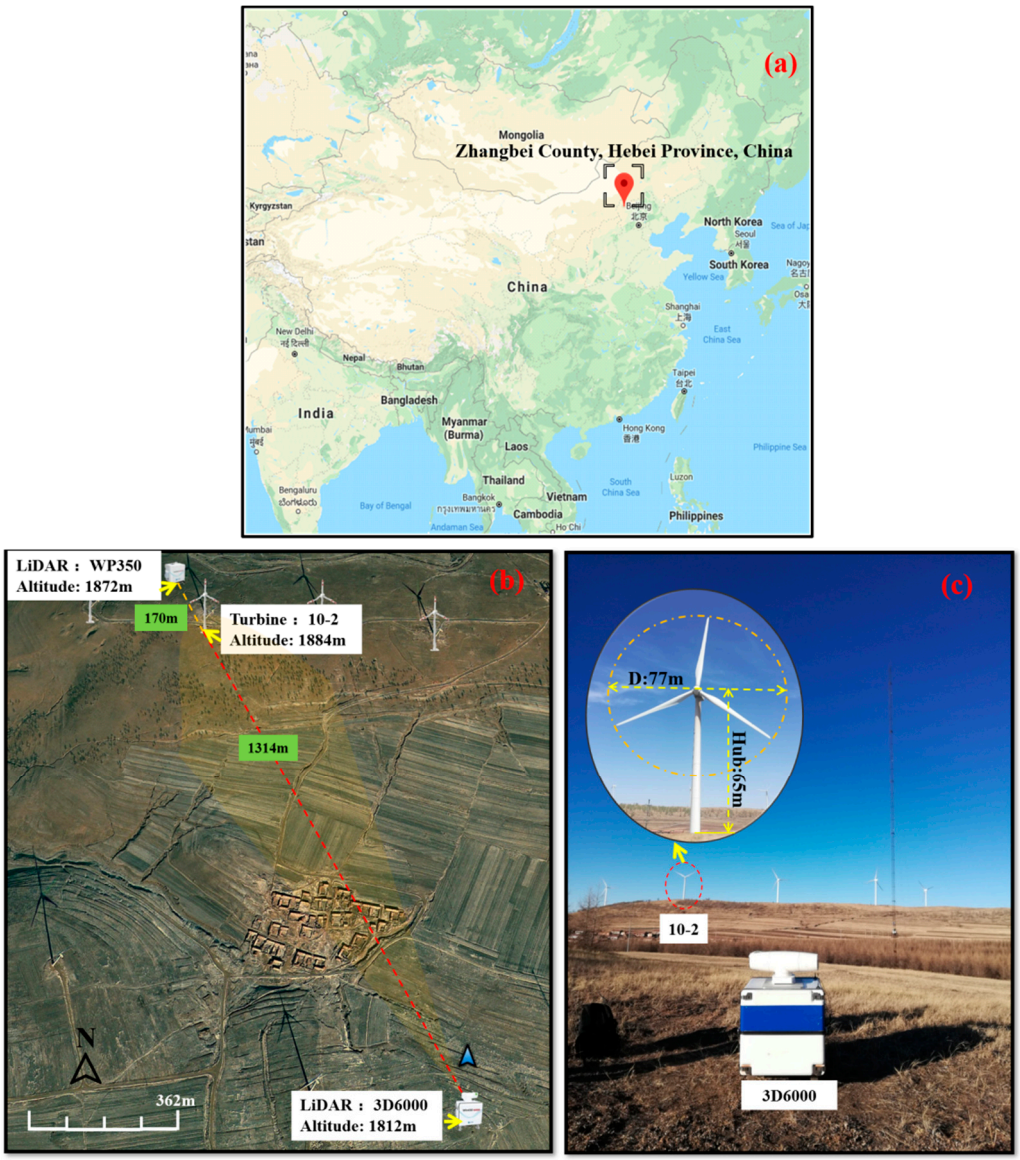

Figure 1. Layout of field measurements: (**a**) experimental site; (**b**) experimental layout shown by Google Maps; (**c**) field layout.

The target wind turbine 10-2 is located at the northern edge of the wind farm. There is no wind turbine wake interference within a range of 1000 m upwind and downwind, which is suitable for wind turbine wake observation. By analyzing the data of the wind measurement tower provided by the wind farm in the past three years, it is concluded that the prevailing wind direction during the experimental period is northwest [34]. Based on this, WP350 is located 170 m northwest of the wind turbine to provide the incoming wind data and 3D6000 is located 1314 m southeast of the turbine 10-2, which ensures that the RHI mode can accurately obtain the turbine 10-2 wake data under the prevailing wind direction. At the same time, it can be seen from Figure 2 that the connecting distance between 3D6000 and turbine 10-2 is 1314 m (about 17D, D is the rotor diameter of the wind turbine, 77

m) and the maximum altitude difference between the two is 87 m, which is suitable for observing the characteristics of wake development under the influence of topographic effects. In addition, in order to obtain the high-resolution incoming wind profile and wake speed distribution as accurately as possible, the measurement heights of WP350 are from 65 m to 350 m above the ground with an interval of 10 m, and the radial range resolution of 3D6000 is set to 20 m (Range Resolution, the minimum distance that line segment AB can distinguish along the projection direction of the LiDAR beam on the ground), which can be seen in Table 1 for the setting parameters of two LiDAR methods in this experiment.

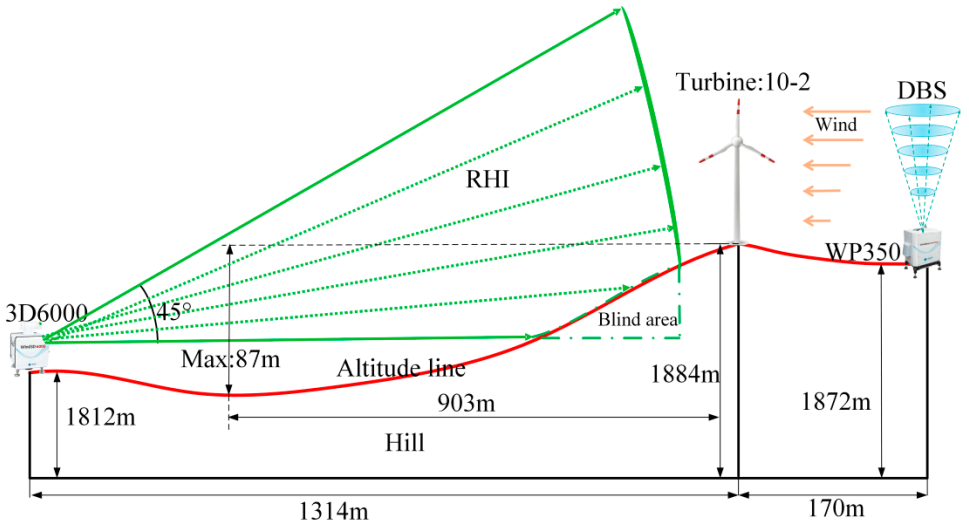

Figure 2. Experimental scheme under conditions where the prevailing wind direction is northwest.

Table 1. Setting parameters of two LiDAR methods in this experiment.

Parameters	DBS mode of WP350	RHI mode of 3D6000
Wave length	1550 nm	1550 nm
Detection range	65 m–350 m	45 m–2000 m
Range resolution	10 m	20 m
Elevation	71°	0–45°
Azimuth	0–360°	330°–340°
Scanning speed	—	1 °/s
Data updating frequency	1 Hz	1 Hz
Wind speed error	≤0.1 m/s	≤0.1 m/s
Wind direction error	≤3°	≤3°
SNR threshold	10	10
Wind speed range	−37.5~+37.5 m/s	−37.5~+37.5 m/s

3. Results and Discussions

3.1. Inflow Wind Profiles and Wake Characteristics in Vertical Height Plane

The inflow wind profile under two different incoming wind conditions are shown in Figure 3a,b, respectively (Case 1: u_0 = 8.69 m/s, I_0 = 9.2%; Case 2: u_0 = 9.35 m/s, I_0 = 11%, and the meaning of these abbreviations can be found in Appendix B). It can be checked that with the increase of altitudes, the wind speed increased. However, the trends are different, which produce two different incoming wind profile shapes and thus, have different effects on the wake profiles. The impact of incoming wind profiles on wake velocity distribution is shown in Figures 4 and 5 with corresponding analysis.

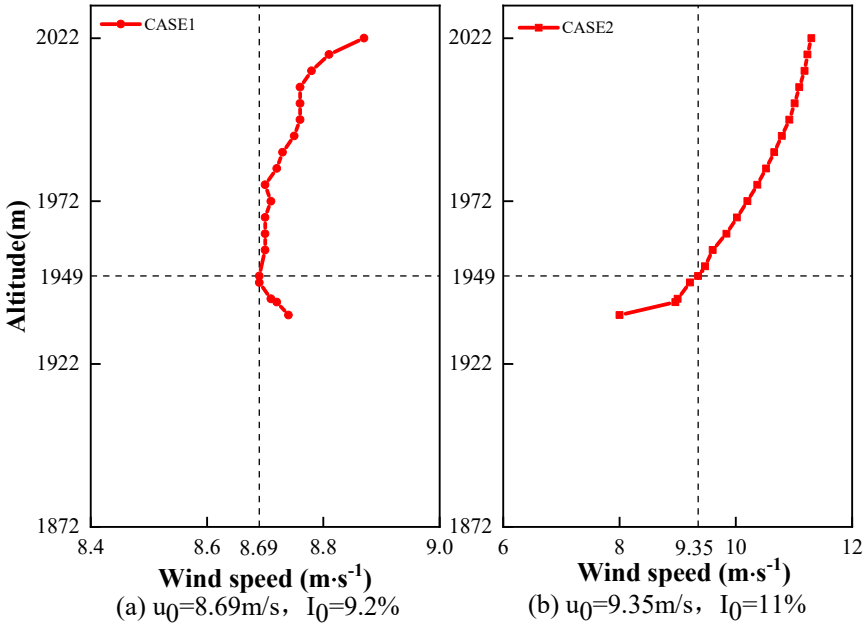

Figure 3. Wind profiles of inflow: (**a**) inflow wind profile of turbine 10-2 in CASE 1; (**b**) inflow wind profile of turbine 10-2 in CASE 2.

Due to the existence of the wind shear effect, the incoming wind speed for the two cases increases with the height away from the ground. In addition, the incoming wind speed and turbulence intensity at hub height of Case 2 in Figure 3b are significantly higher than those of Case 1 in Figure 3a. The corresponding wind shear effect is also more obvious, which is approximately exponentially distributed. Considering the effects of complex terrain and high altitude, the wind shear effect measured in this experiment is significant.

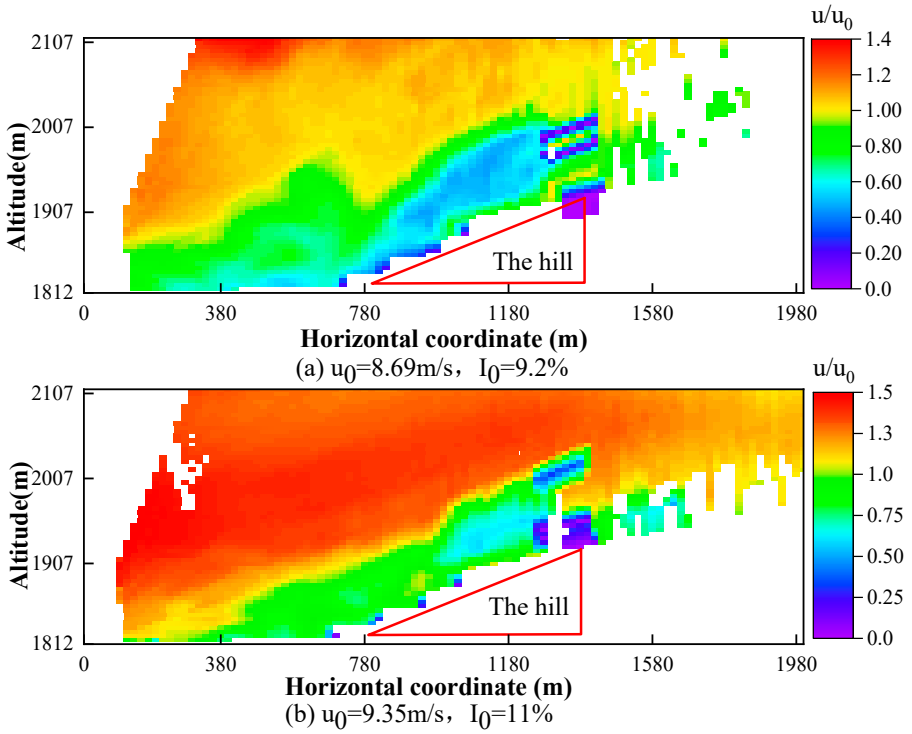

Figure 4. Wind speed profile in vertical height plane: (**a**) cloud diagram of horizontal wind speed distribution in case 1; (**b**) cloud diagram of horizontal wind speed distribution in case 2.

The wake distribution of the horizontal wind speed at the vertical height planes under two different incoming wind conditions is shown in Figure 4a,b, respectively. Note that in Figure 4, there is no wind data in red triangle area due to the occlusion of the ridge and the laser beam emitted by the LiDAR. The wind turbine is located at a position of 1314 m, and the vertical axis represents the altitude. The wake behind the turbine is obvious and a recovery is observed with the increase of the downwind distance.

Meanwhile, under the influence of wind shear effects, it can be observed that the wind speed distribution at different downwind distances of the wind turbine exhibits asymmetrical distribution characteristics. At a certain downwind position, it can be initially observed that the wake speed on the vertical height plane gradually increases in the upward direction of the wake center and decreases gradually in the downward direction. In addition, the wake center sinks as the slope goes down.

To quantify the characteristics of wind speed distribution in the vertical height plane, the wind speed distribution curves at several typical locations in the wake region of the turbine 10-2 is shown in Figure 5. Note that the measurement time of the two conditions (Case 1 and Case 2) is different, that is, the atmospheric conditions are also different, and the effective data obtained by LiDAR 3D6000 are slightly different. In order to intercept the effective and sufficient wind speed data points, different downwind positions are selected for the two wind conditions while ensuring that there are typical location points in the wake area (such as location in near wake area: 2D, location in transition area: 4D, location in far wake area: 12D). It can be seen that although the inflow wind speed of the two conditions is different, under the influence of wind shear effect, the two conditions are similar in the characteristics of wind speed distribution in the wake area, and both of which are non-asymmetric (the axis is referred to wake centerline at each position in the wake region).

At different downwind distances, the wake speed gradually increased in the upward range of the wake center, and the downward range of the wake center showed a trend of increasing first and then decreasing, especially from 2D to 6D. This phenomenon disappears with the downwind distance increase, which means that with the increase of the downwind distance of turbine, the wake effect gradually weakened. After 8D, the wake center gradually disappeared and the wake speed distribution began to approximate the incoming wind profile.

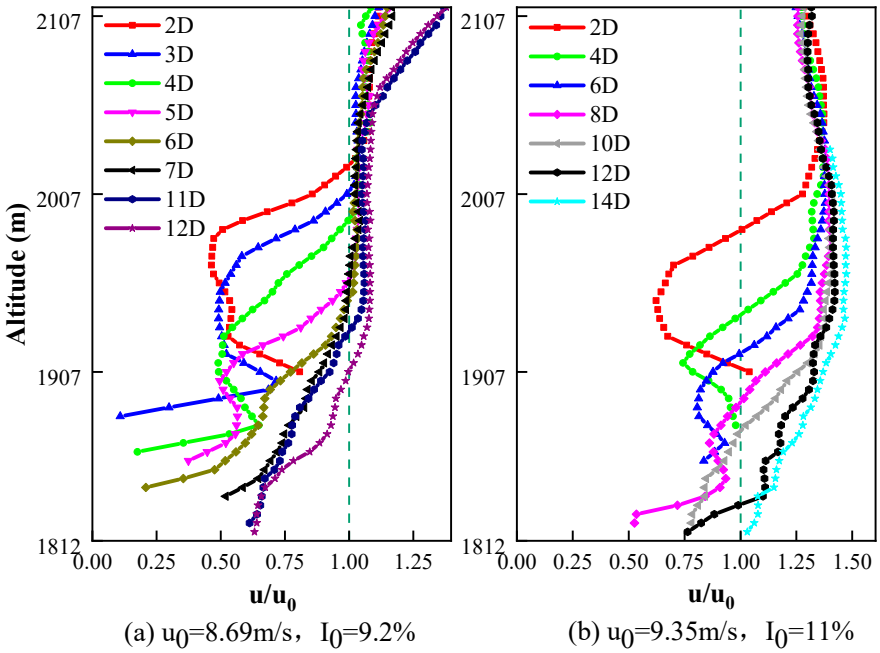

Figure 5. Wind speed distribution in vertical height plane at different downwind locations.

Two main reasons relate to these outcomes: (1) Due to the wind shear effect, the incoming wind profile exhibits an exponential distribution, and because the wind turbine impeller is a symmetrical rotating body, the wind speed in the wake region shows an asymmetric distribution. At the upward wake boundary, the incoming wind speed gradually recovers, and the wind speed in this area will gradually show a trend consistent with the incoming wind profile. (2) At the downward wake boundary, caused by the wind turbine blade rotation, the tower shadow effect as well as the ground friction, the characteristics of wind speed distribution in wake region is more complicated. In the wake boundary, the wind speed gradually increases due to the momentum exchange caused by the wind turbine blade rotation. However, outside the wake boundary, the wind speed gradually decreases due to the weakening of momentum exchange and the influence of factors such as the tower shadow effect and ground friction.

3.2. Topographic Effects on Wake Subsidence

In flat terrain wind farms and offshore wind farms, due to the small effect of wind shear, many scholars assume that the wake speed exhibits a self-similar Gaussian distribution in the research of the wake characteristics, which means that the wake centerline is near the hub height [35,36]. However, in complex terrain wind farms, especially those with large elevation differences, the topography fluctuation will make the wake center sink, and then change the distribution of wind speed in the wake area. In our experiment, there is a slope down behind the turbine and the altitude difference between the 3D6000 and the wind turbine is 77 m. The slope is 10° ($\tan\alpha$ = H/L). Observing from Figures 4 and 5, the center of the wake sinks significantly along the ridge. To characterize the relationship between the descending height of the wake center and the altitude drop caused by the terrain effect, the centerline of the wake is captured. Figure 6 shows the altitude differences between the wake centerline of turbine 10-2 and 3D6000. The solid red line in the figure is the altitude measured by Google Maps which is also the surface of the hill behind the turbine. The black dashed line is the imaginary line of turbine's hub heights. It can be concluded that the altitude line is translated upward by 65 m, which is the hub height of the turbine.

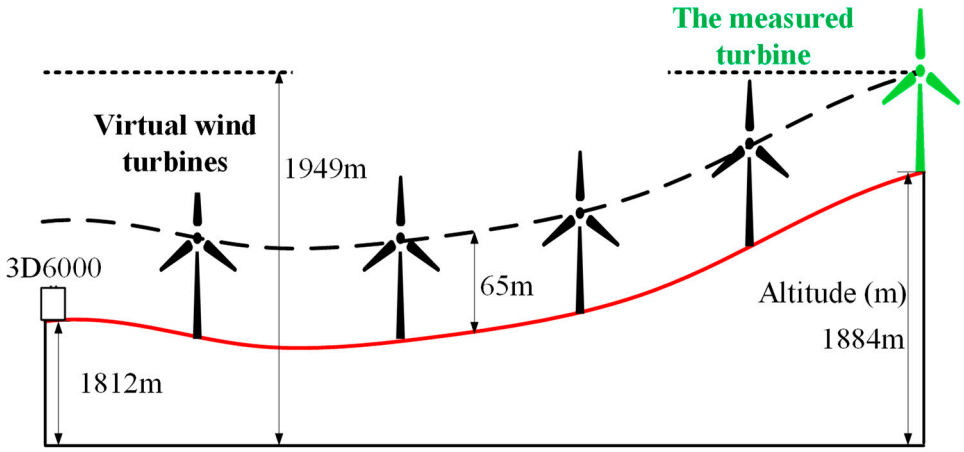

Figure 6. Map of altitude and hypothetical wind turbine's hub heights.

Figure 7 shows the relationship between the measured wake center altitude, the theoretical center wake altitude and the altitude line under the two different cases. The orange dotted line is the theoretical wake center altitude line in flat terrain which means there is no wake subsidence. Meanwhile, the altitudes of wake center at different downwind distance (4D, 6D, 8D, 10D for Case 1 and 3D, 5D 6D for Case 2) of the wind turbine were intercepted from Figure 5 to compare with the theoretical wake center altitudes and the imaginary wind turbine hub center altitude line. Comparison results show that as the altitude difference (altitude difference = wind turbine altitude - altitude line

heighted in red) gradually increases, the sinking height of the wake center of Case 1 and Case 2 also increases accordingly, which is approximately linear with the altitude difference line.

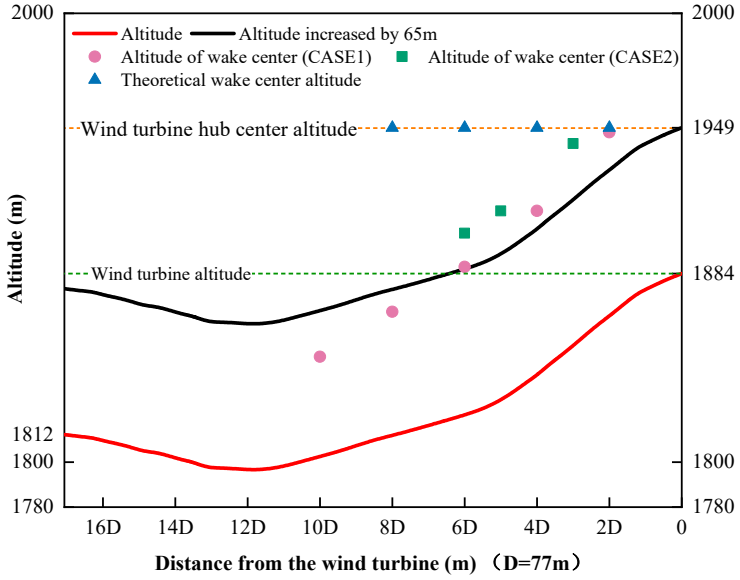

Figure 7. Analysis of the sinking height of the wake center.

To make it clearer, Figure 8 shows the altitude differences at different downwind distances. In Case 2, the maximum altitudes difference occurs at 10D, which is about 20 m. At 6D, the descending height of the wake center is basically consistent with the corresponding altitude difference. In addition, sinking trend in Case 1 was basically consistent with that in Case 2. Based on the above analysis, it can be concluded that the sinking height of the wake center in the complex terrain wind farm has a linear correlation with the altitude difference.

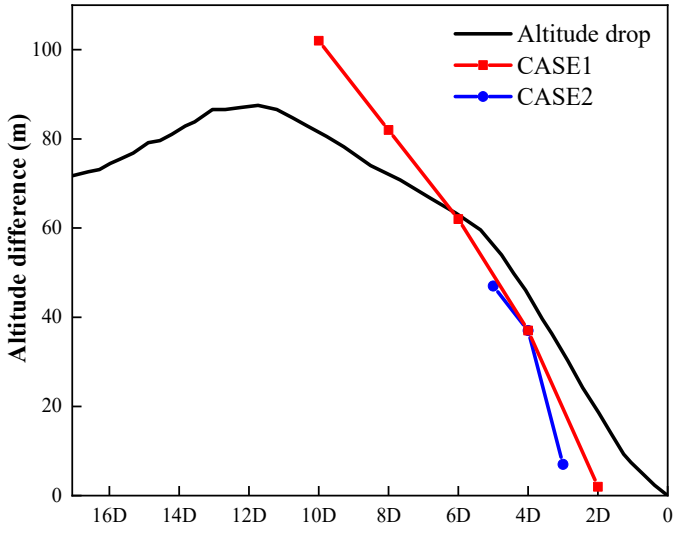

Figure 8. The relationship between the sinking height of the wake center and the altitude difference.

3.3. Analysis of Factors Affecting Wake Recovery Rate

In Sections 3.1 and 3.2, the influence of wind shear effect on wake speed distribution shape and the influence of topography on wake subsidence are analyzed, respectively. In this part, the effect of incoming wind conditions on wake recovery rate is further explored. Figure 9 shows the recovery rate of wake center at different positions in the wake region of turbine 10-2 under the two Cases (Inflow conditions: I_0 = 9.2%, C_T = 0.79 in Case 1 and I_0 = 11%, C_T = 0.68 in Case 2). It can be seen that the

wake recovery rate of Case 2 is significantly higher than that of Case 1 and the difference between the two cases gradually decreases as the increase of the downwind distance. Regarding the explanation of wake recovery phenomenon, classical literature [37] pointed out that the turbulence in wake region could accelerate the wake recovery rate, which was generated due to the convection of wake and free incoming wind. Based on the above analysis, it can be concluded that the turbulence intensity in the wake region of Case 2 is higher than that of Case 1.

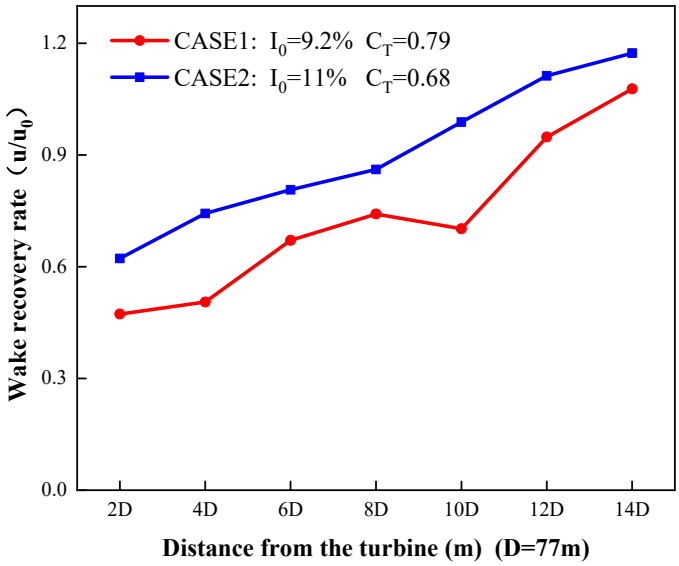

Figure 9. The recovery rate of wake under different inflow conditions.

However, the above is only a preliminary analysis based on the wake theory that the turbulence intensity in the wake region can speed up the recovery of the wake. In the work of Ishihara et al. [38], its wind tunnel experiment shows that when the ambient turbulence intensity I_0 is the same, the larger the thrust coefficient C_T is, the faster the wake recovery rate is; otherwise, when the C_T is the same, the larger the I_0 is, the faster the wake recovery rate becomes. It is interesting that when analyzing the incoming flow information of the two Cases obtained in this experiment, it is found that C_T of Case 1 is greater than Case 2, but I_0 is less than Case 1, which mean that the turbulence intensity in the wake region (I_w) may be jointly determined by I_0 and C_T.

In addition, empirical formulas about the calculation of I_w were proposed by Quarton and Ainslie [39] through wind tunnel tests and then were improved by Hassan [40], based on Formula (1) and Formula (2). It is not difficult to observe that for the determined downwind position, the formulas have the same variables: axial thrust coefficient C_T and incoming turbulence intensity I_0, and have the same proportion. Therefore, it can be initially concluded that the wake recovery rate is determined comprehensively by the turbulence intensity of the incoming flow and the thrust coefficient of the wind turbine again.

To prove this, the turbulence intensities inside the wake I_w in Case 1 and Case 2 are calculated using Formula (2). Results show that the calculated value of the turbulence intensity in wake region in the Case 2 is always higher than that in Case 1, which can be seen in Figure 10. Meanwhile, the turbulence intensity difference between the two Cases gradually decreases with the increasing of the downwind distance. Thus, the different wake recovery rates of these two Cases in Figure 9 can be effectively explained.

$$I_{wake} = \sqrt{I_0{}^2 + \left[4.8 C_T{}^{0.7} I_0{}^{0.68} (x/x_n)^{-0.57}\right]^2} \quad (1)$$

$$I_{wake} = \sqrt{I_0{}^2 + \left[5.7 C_T{}^{0.7} I_0{}^{0.68} (x/x_n)^{-0.96}\right]^2} \quad (2)$$

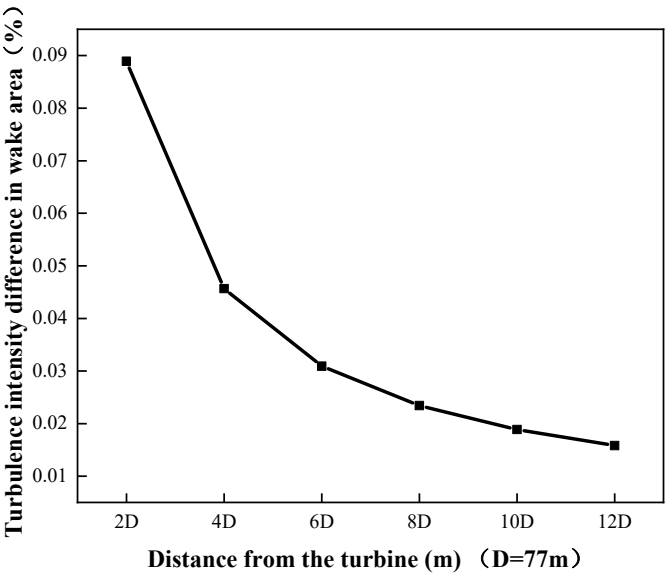

Figure 10. Difference of turbulent intensity in the wake region in Case 2 and Case 1 (Case 2∓Case 1).

4. Conclusions

In this paper, two different LiDAR types are used to experimentally study the wake characteristics in complex terrain wind farms. The characteristics of wake speed distribution in vertical plane under the influence of wind shear effects, the relationship between topographic effects and the wake subsidence as well as the influence of incoming wind characteristics on wake recovery rate were analyzed. Conclusions are summarized as follows:

1. Considering that most field experiments and wake models do not consider the effect of incoming wind shear on the wake field in the study of wake characteristics, this paper uses field data obtained two LiDAR models to analyze the characteristics of wind speed distribution in wake regions under the wind shear effect. Results show that the wake profiles in a wake region are affected by the wind shear effects, which shows an asymmetrical distribution. In addition, the wind speed gradually increases above the wake center, and increases firstly and then decreases under the wake center due to the effect of tower shadow and ground friction.
2. The wake velocity distribution obtained from the RHI model shows that the wake centerline subsidence affected by the topographic effects, and the sinking height of the wake center is linearly related to the altitude drop under the two Cases.
3. By comparing the wake recovery rates in two different conditions, it is verified that the wake recovery rate is affected by the turbulence intensity in the wake region. The greater the turbulence intensity in the wake region, the faster the wake recovery rate. In addition, results show that the turbulence intensity in the wake region is determined by the turbulence intensity of the incoming flow and the thrust coefficient of the wind turbine.
4. Compared with previous complex terrain LiDAR measurement experiments, this study uses two different types of LiDAR models: WP350 for measuring incoming wind conditions and the LiDAR 3D6000 for acquiring wake data. Based on the experimental data, both the characteristics of wake distribution under the influence of terrain and influence of incoming wind conditions on the characteristics of wake development are analyzed, which can provide some guidance for future LiDAR measurement campaign and wind turbine layout optimization.
5. Based on the results provided in this paper, it can be concluded that for specific wind turbines in a complex wind farm, the incoming wind conditions caused by the terrain and altitudes as well as the incoming wind of upstream turbine are different. Thus, specific pitch/yaw control

strategies should be applied for specific turbines to improve the aerodynamic performance of the downwind wind turbines, which should be further investigated.

Author Contributions: Methodology, J.Y.; investigation, Y.G. and T.W.; data curation, T.W.; writing—original draft preparation, F.Z.; supervision, X.G.; funding acquisition, X.G. All authors have read and agreed to the published version of the manuscript.

Funding: This research was funded by the National Natural Science Foundation of China, grant number No.51606068; the Natural Science Foundation of Hebei Province, grant number No.E2019502072; the Fundamental Research Funds for the Central Universities, grant number 2018MS101; the Research Institute for Sustainable Urban Development (RISUD), grant number BBW8; and the FCE Dean Research project of The Hong Kong Polytechnic University, grant number ZVHL.

Conflicts of Interest: The authors declare no conflict of interest. The funders had no role in the design of the study; in the collection, analyses, or interpretation of data; in the writing of the manuscript or in the decision to publish the results.

Appendix A. Inversion Algorithm of Horizontal Wind Speed

Appendix A.1. Doppler Beam Swing (DBS) Model Inversion Algorithm

Step 1: Assuming that the radial wind speed in the five directions of North, East, South, West and Vertical is represented by V_{losN}, V_{losE}, V_{losS}, V_{losW}, V_{losZ}, respectively. And assuming that the north-south water bisection is u, the East-West horizontal component is v, and the vertical component is w, elevation θ is the angle between the laser beam and the horizontal plane. And V is the horizontal wind speed.

Step 2: Calculate the u, v

$$\begin{cases} V_{losN} = u\cos\theta + w\sin\theta \\ V_{losE} = v\cos\theta + w\sin\theta \\ V_{losS} = -u\cos\theta + w\sin\theta \\ V_{losW} = -v\cos\theta + w\sin\theta \\ V_{losZ} = w \end{cases} = \begin{cases} u = \frac{V_{losN} - V_{losS}}{2\cos\theta} \\ v = \frac{V_{losE} - V_{losW}}{2\cos\theta} \\ w = \frac{V_{losN} + V_{losS} + V_{losE} + V_{losW}}{4\sin\theta} \end{cases} \quad \text{(A1)}$$

Step 3: Calculate the horizontal speed V

$$V = \sqrt{\overline{u}^2 + \overline{v}^2} \quad \text{(A2)}$$

Appendix A.2. Range Height Indicator (RHI) Model Inversion Algorithm

Step 1: Assuming that the horizontal wind speed is V and the radial velocity measured by the laser beam is V_{los}. Δθ is the angle between the azimuth angle of the radial beam in RHI mode and the prevailing wind direction, and φ is the pitch angle of the radial beam.

Step 2: Calculate the horizontal speed V

$$V = \frac{V_{Los}}{\cos(\Delta\theta) \cdot \cos(\phi)} \quad \text{(A3)}$$

Appendix B. List of Symbols and Abbreviation

List of symbols and abbreviation

LiDAR	Light Detection and Ranging	D	The rotor diameter (m)
WP350	WindMast WP350	u_0	Incoming wind speed at hub height (m/s)
3D6000	Wind3D6000	I_0	Inflow turbulence intensity at hub height
DBS	Doppler beam Swing	C_T	Thrust coefficient
RHI	Range-Height-Indicator	I_{wake}	Turbulence intensity in wake region
PPI	Plan-Position-Indicator	LOS	Line-of-sight (velocity)
SNR	*Signal-Noise ratio*		
SCADA	Supervisory Control And Data Acquisition		
SLPIV	Super-large-scale particle image velocimetry		

References

1. Astolfi, D.; Castellani, F.; Terzi, L. A study of wind turbine wakes in complex terrain through rans simulation and scada data. *J. Solar Energy Eng.* **2018**, *140*, 9. [CrossRef]
2. Barthelmie, R.J.; Hansen, K.S.; Frandsen, S.T.; Rathmann, O.; Schepers, J.G.; Schlez, W.; Phillips, J.; Rados, K.; Zervos, A.; Politis, E.S.; et al. Modelling and measuring flow and wind turbine wakes in large wind farms offshore. *Wind Energy* **2009**, *12*, 431–444. [CrossRef]
3. Meng, H.; Lien, F.-S.; Li, L. Elastic actuator line modelling for wake-induced fatigue analysis of horizontal axis wind turbine blade. *Renew. Energy* **2018**, *116*, 423–437. [CrossRef]
4. Han, X.; Liu, D.; Xu, C.; Zhong, S.W. Atmospheric stability and topography effects on wind turbine performance and wake properties in complex terrain. *Renew. Energy* **2018**, *126*, 640–651. [CrossRef]
5. Jensen, N.O. *A Note on Wind Generator Interaction*; Risø National Laboratory: Roskilde, Denmark, 1983.
6. Frandsen, S.; Barthelmie, R.; Pryor, S.; Rathmann, O.; Larsen, S.; Højstrup, J.; Thøgersen, M. Analytical modelling of wind speed deficit in large offshore wind farms. *Wind Energy* **2006**, *9*, 39–53. [CrossRef]
7. Tian, L.; Zhu, W.; Shen, W.; Zhao, N.; Shen, Z. Development and validation of a new two-dimensional wake model for wind turbine wakes. *J. Wind Eng. Ind. Aerodyn.* **2015**, *137*, 90–99. [CrossRef]
8. Gao, X.; Yang, H.; Lu, L. Optimization of wind turbine layout position in a wind farm using a newly-developed two-dimensional wake model. *Appl. Energy* **2016**, *174*, 192–200. [CrossRef]
9. Sun, H.; Yang, H. Study on an innovative three-dimensional wind turbine wake model. *Appl. Energy* **2018**, *226*, 483–493. [CrossRef]
10. Barthelmie, R.J.; Pryor, S.C. An overview of data for wake model evaluation in the Virtual Wakes Laboratory. *Appl. Energy* **2013**, *104*, 834–844. [CrossRef]
11. Grassi, S.; Junghans, S.; Raubal, M. Assessment of the wake effect on the energy production of onshore wind farms using GIS. *Appl. Energy* **2014**, *136*, 827–837. [CrossRef]
12. Xydis, G.; Koroneos, C.; Loizidou, M. Exergy analysis in a wind speed prognostic model as a wind farm sitting selection tool: A case study in Southern Greece. *Appl. Energy* **2009**, *86*, 2411–2420. [CrossRef]
13. Castellani, F.; Astolfi, D.; Mana, M.; Piccioni, E.; Becchetti, M.; Terzi, L. Investigation of terrain and wake effects on the performance of wind farms in complex terrain using numerical and experimental data. *Wind Energy* **2017**, *20*, 1277–1289.
14. Jha, P.K.; Duque, E.P.N.; Jessica, L.; Bashioum, J.L.; Schmitz, S. Unraveling the mysteries of turbulence transport in a wind farm. *Energies* **2015**, *8*, 6468–6496. [CrossRef]
15. Nandi, T.N.; Herrig, A.; Brasseur, J.G. Non-steady wind turbine response to daytime atmospheric turbulence. *Philos. Trans. R. Soc. A Math. Phys. Eng. Sci.* **2017**, *375*, 20160103. [CrossRef] [PubMed]
16. Churchfield, M.J.; Lee, S.; Michalakes, J.; Moriarty, P.J. A numerical study of the effects of atmospheric and wake turbulence on wind turbine dynamics. *J. Turbul.* **2012**. [CrossRef]
17. Murali, A.; Rajagopalan, R. Numerical simulation of multiple interacting wind turbines on a complex terrain. *J. Wind Eng. Ind. Aerodyn.* **2017**, *162*, 57–72. [CrossRef]
18. Hyvärinen, A.; Segalini, A. Effects from complex terrain on wind-turbine performance. *J. Energy Resour. Technol.* **2017**, *139*, 051205. [CrossRef]
19. Dou, B.; Guala, M.; Lei, L.; Zeng, P. Experimental investigation of the performance and wake effect of a small-scale wind turbine in a wind tunnel. *Energy* **2019**, *166*, 819–833. [CrossRef]

20. Iungo, G.V. Experimental characterization of wind turbine wakes: Wind tunnel tests and wind LiDAR measurements. *J. Wind Eng. Ind. Aerodyn.* **2016**, *149*, 35–39. [CrossRef]
21. Tian, W.; Ozbay, A.; Hu, H. An experimental investigation on the aeromechanics and wake interferences of wind turbines sited over complex terrain. *J. Wind Eng. Ind. Aerodyn.* **2018**, *172*, 379–394. [CrossRef]
22. Singh, R.K.; Ahmed, M.R. Blade design and performance testing of a small wind turbine rotor for low wind speed applications. *Renew. Energy* **2013**, *50*, 812–819. [CrossRef]
23. Talavera, M.; Shu, F. Experimental study of turbulence intensity influence on wind turbine performance and wake recovery in a low-speed wind tunnel. *Renew. Energy* **2017**, *109*, 363–371. [CrossRef]
24. Li, Q.A.; Maeda, T.; Kamada, Y.; Mori, N. Investigation of wake characteristics of a Horizontal Axis Wind Turbine in vertical axis direction with field experiments. *Energy* **2017**, *141*, 262–272. [CrossRef]
25. Böhme, G.S.; Fadigas, E.A.; Gimenes, A.L.V.; Tassinari, C.E.M. Wake effect measurement in complex terrain—A case study in Brazilian wind farms. *Energy* **2018**, *161*, 277–283. [CrossRef]
26. Subramanian, B.; Chokani, N.; Abhari, R.S. Aerodynamics of wind turbine wakes in flat and complex terrains. *Renew. Energy* **2016**, *85*, 454–463. [CrossRef]
27. Abraham, A.; Dasari, T.; Hong, J. Effect of turbine nacelle and tower on the near wake of a utility-scale wind turbine. *J. Wind Eng. Ind. Aerodyn.* **2019**, *193*, 103981. [CrossRef]
28. Torres Garcia, E.; Aubrun, S.; Coupiac, O.; Girard, N.; Boquet, M. Statistical characteristics of interacting wind turbine wakes from a 7-month LiDAR measurement campaign. *Renew. Energy* **2019**, *130*, 1–11. [CrossRef]
29. Kumer, V.-M.; Reuder, J.; Dorninger, M.; Zauner, R.; Grubišić, V. Turbulent kinetic energy estimates from profiling wind LiDAR measurements and their potential for wind energy applications. *Renew. Energy* **2016**, *99*, 898–910. [CrossRef]
30. Vasiljević, N.; Palma, J.M.L.M.; Angelou, N.; Matos, J.C.; Menke, R.; Lea, G.; Mann, J.; Courtney, M.; Ribeiro, L.F.; Gomes, V.M.M.G.C. Perdigão 2015: Methodology for atmospheric multi-Doppler lidar experiments. *Atmos. Meas. Tech.* **2017**, *10*, 3463–3483. [CrossRef]
31. Mann, J.; Angelou, N.; Arnqvist, J. Complex terrain experiments in the New European Wind Atlas, Philos. *TR Soc. A* **2017**, *375*, 20160101. [CrossRef]
32. Gao, X.; Wang, T.; Li, B.; Sun, H.; Yang, H.; Han, Z.; Wang, Y.; Zhao, F. Investigation of wind turbine performance coupling wake and topography effects based on LiDAR measurements and SCADA data. *Appl. Energy* **2019**, *255*, 113816. [CrossRef]
33. Sun, H.; Gao, X.; Yang, H. Validations of three-dimensional wake models with the wind field measurements in complex terrain. *Energy* **2019**, *189*, 116213. [CrossRef]
34. Gao, X.; Li, B.; Wang, T.; Sun, H.; Yang, H.; Li, Y.; Wang, Y.; Zhao, F. Investigation and validation of 3D wake model for horizontal-axis wind turbines based on filed measurements. *Appl. Energy* **2020**, *260*, 114272. [CrossRef]
35. Ge, M.; Wu, Y.; Liu, Y.; Li, Q. A two-dimensional model based on the expansion of physical wake boundary for wind-turbine wakes. *Appl. Energy* **2019**, *233*, 975–984. [CrossRef]
36. Chamorro, L.P.; Porté-Agel, F. A wind-tunnel investigation of wind-turbine wakes: Boundary-layer turbulence effects. *Bound. Layer Meteorol.* **2009**, *132*, 129–149. [CrossRef]
37. Vermeer, L.; Sørensen, J.N.; Crespo, A. Wind turbine wake aerodynamics. *Prog. Aerosp. Sci.* **2003**, *39*, 467–510. [CrossRef]
38. Ishihara, T.; Yamaguchi, A.; Fujino, Y. Development of a new wake model based on a wind tunnel experiment. *Glob. Wind Power* **2004**, *105*, 33–45.
39. Quarton, D.C.; Ainslie, J.F. Turbulence in wind turbine wakes. *Wind Eng.* **1989**, *14*, 15–23.
40. Hassan, U. A wind tunnel investigation of the wake structure within small wind turbine farms. In *ETSU-WN-5113*; Harwell Laboratory: Havel, UK, 1993.